

Field-Induced Lifshitz Transition in the Magnetic Weyl Semimetal Candidate PrAlSi

Lei Wu¹, Huakun Zuo¹, Lingxiao Zhao^{1,2,*}, Yongkang Luo^{1,*}, Zengwei Zhu^{1,*}

(1) *Wuhan National High Magnetic Field Center and School of Physics,
Huazhong University of Science and Technology,
Wuhan 430074, China*

(2) *Department of Physics,
Southern University of Science and Technology,
Shenzhen 518055, China*

(Dated: January 14, 2022)

Lifshitz transition (LT) refers to an abrupt change in the electronic structure and Fermi surface, and is associated to a variety of emergent quantum phenomena. Amongst the LTs observed in known materials, the field-induced LT has been rare and its origin remains elusive. To understand the origin of field-induced LT, it is important to extend the material basis beyond the usual setting of heavy fermion metals. Here, we report on a field-induced LT in PrAlSi, a magnetic Weyl semimetal candidate with localized 4f electrons, through a study of magnetotransport up to 55 T. The quantum oscillation analysis reveals that across a threshold field $B^* \approx 14.5$ T the oscillation frequency ($F_1 = 43$ T) is replaced by two new frequencies ($F_2 = 62$ T and $F_3 = 103$ T). Strikingly, the LT occurs well below quantum limit, with obvious temperature-dependent oscillation frequency and field-dependent cyclotron mass. Our work not only enriches the rare examples of field-induced LTs, but also paves the way for further investigation on the interplay among topology, magnetism and electronic correlation.

The Lifshitz transition (LT) has received renewed attention in the condensed matter physics. A LT [1] is an electronic topological transition of Fermi surface (FS) driven by the variation of the band structure and/or the Fermi energy. Since such a transition does not necessarily require simultaneous symmetry breaking, and meanwhile, it can occur at $T = 0$, tuned by parameters other than temperature (such as pressure, strain, doping, magnetic field etc.)[1, 2], it, therefore, can be deemed as a *topological* quantum phase transition. In the vicinity of Lifshitz transitions, many peculiar emergent phenomena may appear, such as van-Hove singularity, non-Fermi-liquid behavior, unconventional superconductivity and so on (e.g. [3, 4]).

Compared with a number of cases tuned by doping or pressure that have been widely seen in topological systems [5, 6], cuprate superconductors [7, 8], iron pnictides superconductors [9, 10], and other strongly correlated materials [3, 11], the examples of LT driven by magnetic field are rare. This is because the energy scale of a laboratory magnetic field, in the order of 1-10 meV, is much smaller than the characteristic energy scale of most metals ($\sim 10^2 - 10^3$ meV). Only in a few cases, mostly limited in heavy-fermion (HF) metals [12-20], the hybridization between conduction electrons and localized *f* electrons leads to narrow renormalized bands with a small Fermi energy and thus the Zeeman term can be sufficiently strong to shift the spin-split FS [15]. Recently, field-induced LT was also observed in some low Fermi energy non-magnetic semimetals such as bismuth [21], TaP[22] and TaAs[23], wherein magnetic field beyond quantum limit can empty a Dirac or Weyl pocket with small Fermi energy. However, in these cases, no additional Fermi pocket emerges and the carriers of the empty pocket were transferred to other pockets (previ-

ously existing).

Here we present a new example of field-induced LT beyond heavy-fermion systems in the magnetic Weyl semimetal candidate PrAlSi, by a systematic study of quantum oscillation (QO) effect extended to a magnetic field up to 55 T. We observe a single frequency ($F_1 = 43$ T) below a critical field of $B^* = 14.5$ T, in agreement with what was previously reported [24]. Above B^* , we see clearly the emergence of two new frequencies ($F_2 = 62$ T and $F_3 = 103$ T) and the disappearance of the original F_1 . We exclude the possibility of magnetic breakdown and identify B^* as a critical point where the field-induced LT occurs. By comparing the reported Fermi surface of NdAlSi and theoretical calculation of PrAlSi, we conclude that the LT occurs in the hole-like Weyl pockets along the direction of Γ -X of the Brillouin zone (BZ). Our work not only enriches the rare examples of field-induced LTs, but also paves the way for further investigation on the interplay among topology, magnetism and electronic correlation.

The *RAlX* family (*R* = rare earth and *X* = Si or Ge) compounds have recently been proposed to host ideal candidates of magnetic Weyl semimetals[25, 26], and provide a platform to investigate the interaction between magnetism and Weyl physics [27-31]. They crystallize in a tetragonal structure with the noncentrosymmetric space group symmetry of $I4_1/m\bar{d}$ (No. 109). One advantage of this family is that Weyl nodes generated by inversion breaking are robust and shifted by the Zeeman coupling in the *k* space [25]. Several intriguing physical properties have been observed in this family. The list includes the coexistence of type-I and type-II Weyl fermion in LaAlSi [32] and LaAlGe [33], a novel topological Hall effect in CeAlGe[34] and anisotropic anomalous Hall effect in CeAlSi[35], and Weyl-driven collective magnetism

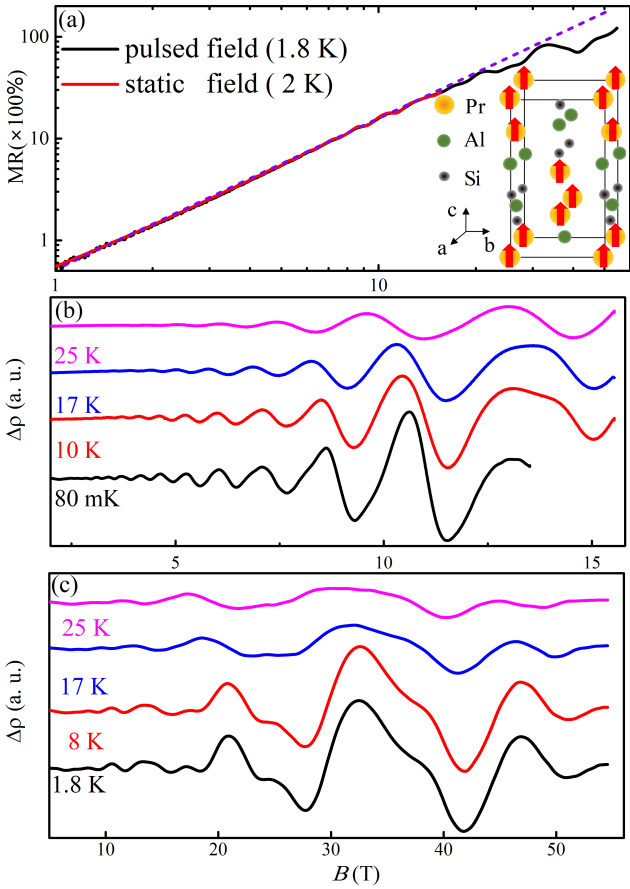


FIG. 1. (a) The field-dependent of MR measured under static field at 2 K and pulsed field at 1.8 K. The inset is crystal structure(I4₁/md) of PrAlSi as the magnetic field easily polarizes the moments of Pr along the *c*-axis. (b) Field dependence of the oscillatory part of magnetoresistance $\Delta\rho(B)$ in low magnetic field measured under static field, showing only a single QO frequency. (c) $\Delta\rho(B)$ in high magnetic field measured by pulsed magnetic field, showing more QO frequencies with a complex pattern.

in NdAlSi [36]. The compound PrAlSi studied here is a ferromagnetic semimetal with Curie temperature $T_C \sim 18$ K. A recent work based on static field (9 T) transport measurements by Lyu et al revealed a large anomalous Hall conductivity $\sim 2000 \Omega^{-1}\text{cm}^{-1}$ and an unusual temperature dependence of QO with a single frequency [24].

High-quality single crystals of PrAlSi were synthesized using the flux method. The inset of Fig. 1(a) shows the crystal structure of PrAlSi with the magnetic moments of Pr easily orientated along *c*-axis after the application of a small field [24]. In our transport measurements, the magnetic field was along the *c*-axis and the electrical current was along the *b*-axis (see more about material and method in supplemental material (SM)). Fig. 1(a) shows magnetoresistance measured in static field at 2 K (red curve) and pulsed magnetic field at 1.8 K (black curve). Normalized magnetoresistance $(\rho(B) - \rho(0))/\rho(0)$ reaches 116 at 55 T and remains non-saturating. The purple dashed line

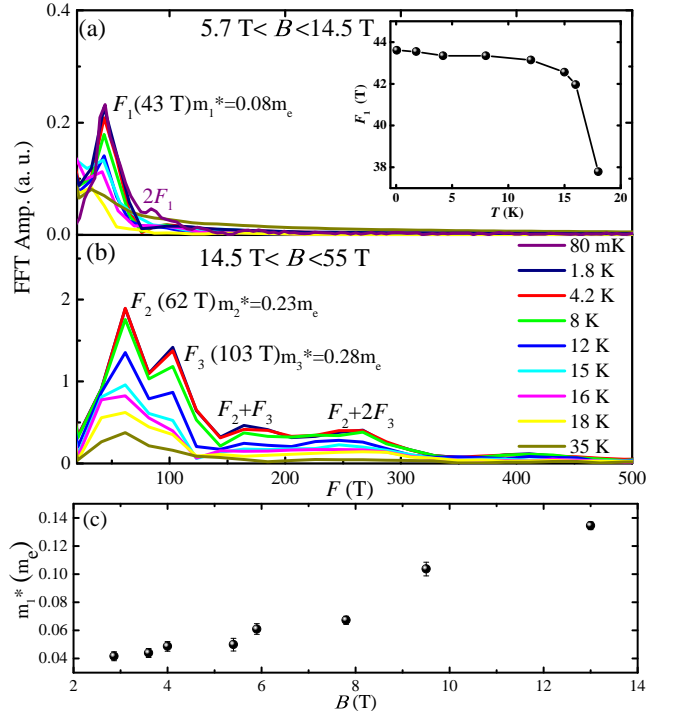


FIG. 2. FFT spectra of SdH oscillations at various temperatures with the magnetic field along *c*-axis. (a) and (b) represent different field ranges which are lower than 14.5 T with only one fundamental frequency and above 14.5 T with another two main higher frequencies and harmonic terms, respectively. The inset shows the temperature-dependent frequency F_1 extracted from (a). (c) The corresponding effective mass of F_1 as a function of magnetic field B .

corresponds to $B^{1.7}$. Fig. 1(b) presents the oscillatory part of the longitudinal resistivity $\Delta\rho(B)$, obtained by subtracting a smoothed background from the measured $\rho(B)$ (see the SM for more raw data). At low temperature, oscillations are visible above the field as low as 3 T, indicating the good quality of the sample. The rough Dingle mobility of $1/B_c = 0.33 \text{ T}^{-1}$ is close to the average mobility of $0.26 \text{ m}^2/\text{Vs}$ yielded from the amplitude of the quadratic low-field magnetoresistance (see the SM). The single-frequency QO for static field measurements retains until temperature down to 80 mK. A more complex pattern emerges when larger magnetic field is applied, as seen in 1(c).

Fig. 2(a) and (b) show the results of the fast Fourier transformation (FFT) of the oscillatory part of the magnetoresistance $\Delta\rho$ as a function of $1/B$. The SdH frequencies extracted from low-field ($B < 14.5$ T) and high-field ($B > 14.5$ T) data display a dramatic difference. Note that, since this compound is ferromagnetic, we took into the demagnetization factor to correct the applied field in all the analysis of SdH effect (see the SM for more details). We identified $B^* = 14.5$ T as a critical field, after checking several fields close to B^* (see more in the SM). There is only one fundamental frequency in the FFT spectrum until down to 80 mK below B^* , see Fig.

2(a). It should be noted that F_1 gradually decreases with temperature, changes from 43 T at 80 mK to 32 T at 35 K, as shown in the inset. Similar temperature dependence in F_1 was also reported in an earlier work on PrAlSi[24], whereas the values of F_1 are relatively smaller than ours. We attribute this discrepancy to some difference in stoichiometry[19].

Fig. 2(b) shows that above B^* there are two new QO frequencies ($F_2 = 62$ T, $F_3 = 103$ T) and their high-order harmonics. Such a change in Fermi surface is also manifested in the effective cyclotron mass m^* . The value of m^* for each frequency can be deduced from the fitting of FFT amplitude according to the temperature damping factor, and this yields the small $m^* = 0.08 m_e$ for F_1 (with field range 5.7-14.5 T), and 0.23 m_e and 0.28 m_e for F_2 and F_3 , respectively, where m_e is the mass of a free electron. Interestingly, a careful look into the temperature dependence of the amplitude of the oscillatory peak leads to the fact that the effective mass is enhanced 3-fold between 2.8 T and B^* , as shown in Fig. 2(c). This feature is reminiscent of HF systems displaying a LT, and will be discussed more later on. More expatiation about effective mass mentioned above is exhibited in SM.

To further demonstrate the field-induced Fermi surface change near $B^* = 14.5$ T, we performed Lifshitz-Kosevich (LK) fitting on $\Delta\rho(B)$. More details can be found in SM. As is shown in Fig. 3(a), the $\Delta\rho$ for field below B^* can be well reproduced by a LK fitting with a single F_1 (cf the red dot line). However, such a fitting collapses when field exceeds B^* . This problem can be fixed in an alternate fitting by employing both F_2 and F_3 , seeing the blue dot line in Fig. 3(b). Noteworthy that this 2-frequency LK fitting fails in the low-field window, implying that F_2 and F_3 appears only in the high-field range.

Thus, the variation of QO frequencies with the disappearance of 43 T and the emergence of 62 T and 103 T clearly point to the change in Fermi surface topology, viz a LT. Firstly, we can rule out magnetic breakdown as the origin, because there is no extra QO frequency (19 T and 60 T) in the low-field range even for temperature as low as 80 mK. Moreover, the frequency peak of 43 T does not persist under high magnetic field, either. Secondly, we can also exclude a metamagnetic transition as the driver of this process. Fig. 4(a) shows the field-dependence of magnetization at 2 K with the magnetic field applied along c -axis. One clearly finds that the magnetization saturates to $\sim 3.1 \mu_B/\text{Pr}$ at a small field 0.48 T, and no additional transition can be resolved nearby 14.5 T except for some traces of de Haas-van Alphen oscillations (inset of Fig. 4(a)). This is different from the case of NdAlSi, where a magnetic transition to the final Weyl-mediated helical magnetism leads to a change in QO frequency [36].

In order to further clarify this field-induced LT, it is helpful to estimate the density of carriers of each Fermi pocket. According to the Lifshitz-Onsager relation, $F = (\hbar/2\pi e)A_F$, where \hbar is Planck's constant and $A_F = \pi k_F^2$ is an extremal cross-sectional area of the Fermi sur-

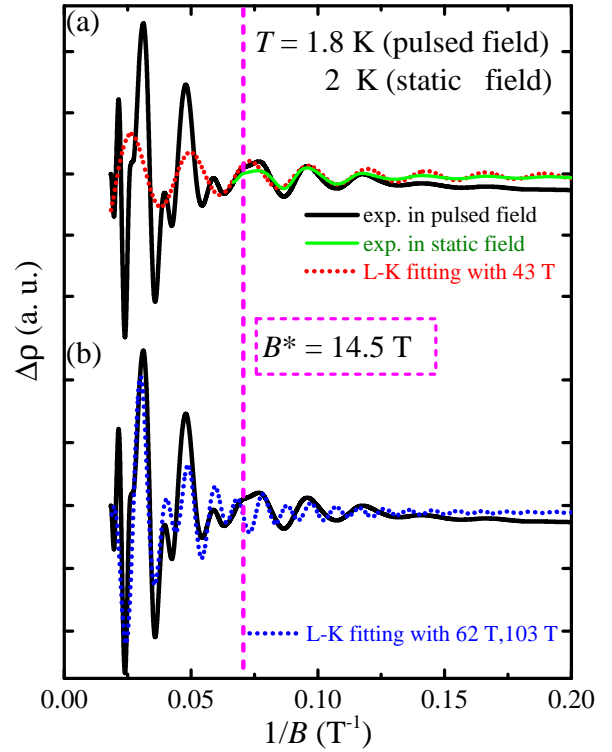


FIG. 3. The Lifshitz-Kosevich fit to $\Delta\rho(B)$. Inverse field dependence of the oscillatory magnetoresistance at 1.8 K up to 55 T and static field at 2 K are depicted as black and green lines, respectively. Note that the L-K fitting with a single frequency of 43 T reproduces the SdH oscillations nicely for field below B^* , but fails for $B > B^*$, as shown in panel (a). A multi-frequency L-K fitting employing both F_2 and F_3 describes $\Delta\rho(B)$ reasonably well for $B > B^*$, seeing panel (b).

face perpendicular to the field with Fermi wave vector k_F . The bands become non-degenerate due to spin-orbit coupling[36]. Assuming these Fermi pockets are spheres, we find that the LT wipes out $n_{F_1} = 3.2 \times 10^{18} \text{ cm}^{-3}$ and produces $n_{F_2} = 5.5 \times 10^{18} \text{ cm}^{-3}$ and $n_{F_3} = 1.2 \times 10^{19} \text{ cm}^{-3}$ per 4 pockets. Note that the total number of pockets would be a multiple of four, due to the symmetric requirement (see below).

The total carrier density of hole and electron can be also extracted by fitting the Hall resistivity to a two-band model, $\rho_{xy}(B) = \frac{B}{e} \frac{(n_h \mu_h^2 - n_e \mu_e^2) + \mu_h^2 \mu_e^2 (n_h - n_e) B^2}{(n_h \mu_h + n_e \mu_e)^2 + \mu_h^2 \mu_e^2 (n_h - n_e)^2 B^2}$. Here, n and μ represent carrier density and mobility, and the subscripts h and e denote hole and electron, respectively. We obtain $n_h = 4.3 \times 10^{19} \text{ cm}^{-3}$, $n_e = 5.3 \times 10^{19} \text{ cm}^{-3}$, $\mu_h = 0.18 \text{ m}^2/\text{Vs}$ and $\mu_e = 0.22 \text{ m}^2/\text{Vs}$. These values fit both Hall resistivity and magnetoresistivity reasonably well up to B^* (see Fig. 4(c) and SM). The deduced mobilities are also close to the value obtained from quantum oscillations and magnetoresistivity. The average zero-field mobility $\langle \mu \rangle$ extracted from the residual resistivity $\rho_0 = 15 \mu\Omega\cdot\text{cm}$ is about $0.5 \text{ m}^2/\text{Vs}$, slightly larger than the finite-field mobility. Such a discrepancy

has been observed in other semimetals[37, 38] and attributed to the field-induced mobility reduction. The carrier densities of hole and electron are within 10% of the compensation $2[n_e n_h / (n_e + n_h)]$, compared to $\sim 4\%$ in bismuth[39] and WTe₂[40]. This near compensation would explain the observed unsaturated magnetoresistance. The slight excess in hole may result from an uncontrollable doping which could be also the reason for the sample dependence of F_1 as discussed above.

This fit, which properly works up to B^* (shown by a black arrow in Fig. 4(c)), fails above B^* . The change occurring at B^* is evident in Fig. 4(b), which shows the first derivative of the longitudinal and Hall resistivities. We let $|n_h - n_e|$ to stay constant across B^* , in order to respect the Luttinger theorem [41]. We infer that F_2 and F_3 should correspond to carriers of opposite signs with a density difference of $|n_{F_3} - n_{F_2}| = 6.5 \times 10^{18} \text{ cm}^{-3}$. Assuming that there are 8 pockets for F_1 ($2n_{F_1} = 6.4 \times 10^{18} \text{ cm}^{-3}$), would be compatible with the Luttinger theorem. Both types of carriers increase by about $0.6 \times 10^{19} \text{ cm}^{-3}$ ($n_{F_3} - 2n_{F_1}$ and n_{F_2} , respectively). Fitting the Hall resistivity curve with $n_h = 4.9 \times 10^{19} \text{ cm}^{-3}$ and $n_e = 5.9 \times 10^{19} \text{ cm}^{-3}$, we obtain $\mu_h = 0.05(1) \text{ m}^2/\text{Vs}$ and $\mu_e = 0.16(1) \text{ m}^2/\text{Vs}$. This is shown in Fig. 4(c) with blue line. The mobility ($\mu = \frac{e\tau}{m^*}$) of holes drop ($\sim 72\%$) more than that of electron ($\sim 27\%$), implying the sign of F_1 with a small mass should be hole-like, since its mass increases by 2.5 times by assuming a same scattering time τ . We conclude that F_2 has an electron-like sign and F_3 is a hole-like one. Thus, each hole pocket (F_1) evolves to a larger hole pocket (F_3) and an additional electron pocket (F_2). This indicates the existence of a van-Hove singularity (saddle point) in this system.

Next, we tried to locate these pockets in the BZ, following the guide of the theoretical calculations of band structure, Weyl nodes and Fermi surface of PrAlSi [42] and our similar calculation results (see the SM). The electronic structure also resembles that of NdAlSi [36]. Since the center of the BZ is not occupied, symmetry imposes four-fold degeneracy of each pocket. We propose the most possible positions of pockets in the BZ as shown in Fig. 4(d). The pockets along Γ –S are large and cannot be easily modified, hence they are not shown in Fig. 4(d). Instead, the bands along Γ –X are shallow and host Weyl points and they should be susceptible to magnetic field. Indeed, some Weyl signatures observed for the pocket F_1 . All the field values extracted from the peak and valley positions of SdH fall on a line with an intercept of ~ 0.01 in the Landau fan diagram, indicating a non-trivial π phase (see the Fig. S5(b)). Its cyclotron mass is very small and changes with magnetic field. Note that a normal parabolic band ($E = \frac{\hbar^2 k^2}{2\pi m}$) would not change its cyclotron mass ($m_{CR} = \frac{\hbar^2}{2\pi} \frac{\partial A_F(E, k_F)}{\partial E}$)[43] as the Fermi energy changes. The new F_2 and F_3 pockets are on the Γ –X line.

Take together, three prominent features about the LT in PrAlSi can be found: (i) the QO frequencies are strongly temperature dependent, (ii) the quasiparticle

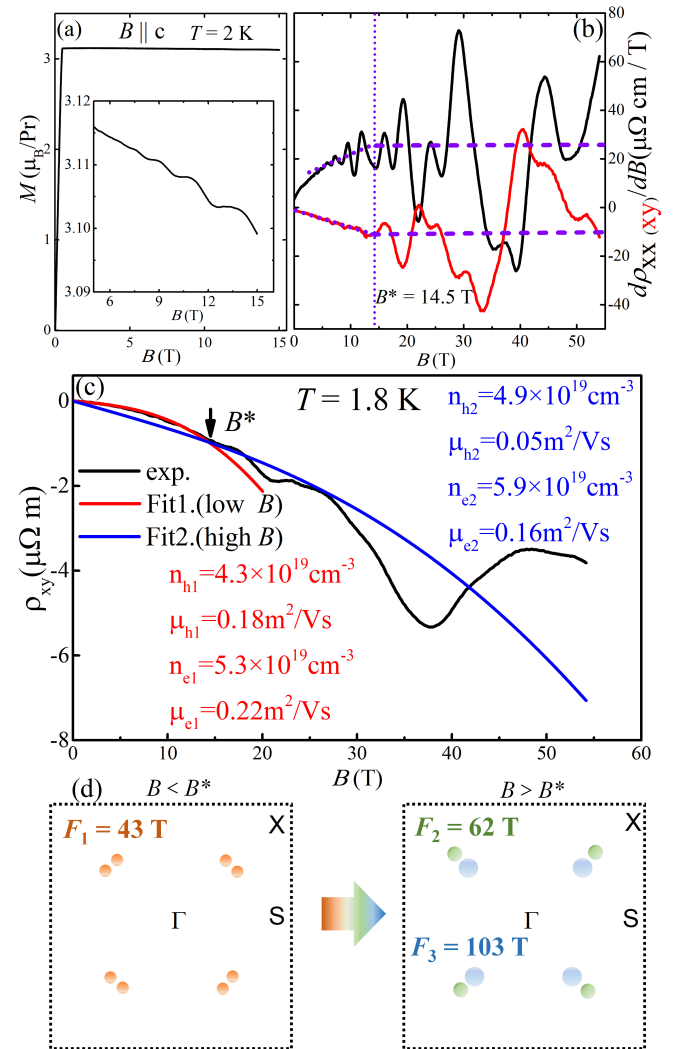


FIG. 4. (a) The magnetization of PrAlSi with the magnetic field applied along the c -axis, the inset is the enlarged part with evident QOs. (b) The black and red lines are the first derivative of the MR and Hall resistivities. The violet dotted lines suggest the change of slopes in both of them at the B^* . (c) The field dependence of Hall resistance at 1.8 K along with two fitting curves with two-band model. The red and blue curves correspond to the fits to the low-field and high-field respectively. (d) Sketch of Lifshitz transition in the BZ. Two tiny hole pockets (in orange) with $F_1 = 43 \text{ T}$ located along the sides of Γ –X transform into one electron pocket in green with $F_2 = 62 \text{ T}$ and one hole pocket in blue with $F_3 = 103 \text{ T}$ after LT, implying the existence of a van-Hove singularity. The pockets along Γ –S are not shown here (see the SM).

effective mass increases gradually when approaching B^* , and (iii) the critical field for such LT is far below quantum limit. In conventional metals, only a small change in QO frequency of the order of $(k_B T/E_F)^2$ is expected upon warming [44]. Temperature-dependent QO frequency was observed in some HF metals, which is typically ascribed to the sensitivity of the f - c (c - conduction elec-

trons) hybridization and the corresponding Kondo resonance state with a variation of temperature[12, 13, 45]. In this framework, the change of m^* was also attributed to a itinerant - localized transition of $4f$ electrons[14]. However, in PrAlSi, DFT calculations manifested that the Pr- $4f$ bands locates well below the Fermi level (see the SM), notable f - c hybridization is unlikely. Furthermore, PrAlSi is a low-carrier density semimetal, the Kondo screening is also expected to be weak according to Nozières exhaustion idea[46, 47]. Therefore, it is unlikely that the observed LT in PrAlSi originates from a competition between Zeeman term and a characteristic Kondo coherence energy as in HF systems. In the cases of bismuth [21], TaP[22] and TaAs[23], the quantum limit has been reached to empty a Dirac or Weyl pocket, and caused a field-induced LT. In our case, however, a rough estimate yields the quantum limit field in the range of 40-100 T, much larger than the critical field $B^* \sim 14.5$ T.

Another possibility for the observed LT in PrAlSi might be related to the crystal-electric-field (CEF) effect. This arises because the nine fold-degenerate $j = 4$ multiplet of Pr^{3+} in a D_{2d} (42m) point symmetry CEF splits into two non-Kramers doublets and five singlets[48]. A recent analysis based on specific heat measurements revealed that the ground state is probably a doublet, while the magnetic entropy gain reaches $R \ln 3$ at about 20 K, $R \ln 4$ at about 30 K, and saturates to $R \ln 9$ at a temperature as low as ~ 95 K[24]. This suggests that at least one excited state sitting not far above the ground doublet, potentially in the order of 10 K. It is reasonable to speculate that magnetic field of ~ 10 T might be sufficient to modify the CEF energy levels and the orbital characters,

which possibly changes the Fermi surface topology. In addition, this field-induced evolution of CEF levels is also qualitatively consistent with the temperature-dependent QO frequency and field dependent m^* as observed experimentally. Actually, this scenario was also proposed recently for the field-induced Fermi surface reconstruction in CeRhIn₅[49]. To further address this possibility, more experiments like inelastic neutron scattering are needed to figure out the diagram of the CEF splitting.

In summary, we grew high quality single crystals and observed pronounced SdH oscillations in PrAlSi with magnetic field up to 55 T. A LT transition occurs around 14.5 T. The change in carrier density and Fermi pockets revealed by QO and Hall effect are consistent with each other. By comparison with theoretical calculations, we propose that LT occurs along the Γ -X orientation and involves the Weyl pockets. One hole pocket becomes an electron pocket and a hole pocket, which indicates the existence of a van-Hove singularity. PrAlSi, therefore, represents a unique case of field-induced LT beyond the HF systems.

We thank Kamran Behnia for insightful discussions. This work is supported by the National Science Foundation of China (Grant Nos. 12004123, 51861135104 and 11574097), the National Key Research and Development Program of China (Grant No. 2016YFA0401704), the Fundamental Research Funds for the Central Universities (Grant no. 2019kfyXMBZ071).

* zhaolx@hust.edu.cn

* mpzslyk@hust.edu.cn

* zengwei.zhu@hust.edu.cn

[1] I. Lifshitz, Sov. Phys. JETP **11**, 1130 (1960).

[2] A. A. Varlamov, Y. M. Galperin, S. G. Sharapov, and Y. Yerin, Low Temperature Physics **47**, 672 (2021).

[3] A. Steppke, L. Zhao, E. Barber Mark, T. Scafidi, F. Jerzembeck, H. Rosner, S. Gibbs Alexandra, Y. Maeno, H. Simon Steven, P. Mackenzie Andrew, and W. Hicks Clifford, Science **355**, eaaf9398 (2017).

[4] Y. Luo, A. Pustogow, P. Guzman, A. P. Dioguardi, S. M. Thomas, F. Ronning, N. Kikugawa, D. A. Sokolov, F. Jerzembeck, A. P. Mackenzie, C. W. Hicks, E. D. Bauer, I. I. Mazin, and S. E. Brown, Phys. Rev. X **9**, 021044 (2019).

[5] H. F. Yang, L. X. Yang, Z. K. Liu, Y. Sun, C. Chen, H. Peng, M. Schmidt, D. Prabhakaran, B. A. Bernevig, C. Felser, B. H. Yan, and Y. L. Chen, Nature Communications **10**, 3478 (2019).

[6] Y. Liu, Y.-F. Liu, X. Gui, C. Xiang, H.-B. Zhou, C.-H. Hsu, H. Lin, T.-R. Chang, W. Xie, and S. Jia, Proceedings of the National Academy of Sciences **117**, 15517 (2020).

[7] S. Benhabib, A. Sacuto, M. Civelli, I. Paul, M. Cazayous, Y. Gallais, M. A. Méasson, R. D. Zhong, J. Schneeloch, G. D. Gu, D. Colson, and A. Forget, Physical Review Letters **114**, 147001 (2015).

[8] M. R. Norman, J. Lin, and A. J. Millis, Physical Review B **81**, 180513 (2010).

[9] M. Ren, Y. Yan, X. Niu, R. Tao, D. Hu, R. Peng, B. Xie, J. Zhao, T. Zhang, and D.-L. Feng, Science Advances **3**, e1603238 (2017).

[10] C. Liu, T. Kondo, R. M. Fernandes, A. D. Palczewski, E. D. Mun, N. Ni, A. N. Thaler, A. Bostwick, E. Rotenberg, J. Schmalian, S. L. Bud'ko, P. C. Canfield, and A. Kaminski, Nature Physics **6**, 419 (2010).

[11] J. Kwon, M. Kim, D. Song, Y. Yoshida, J. Denlinger, W. Kyung, and C. Kim, Physical Review Letters **123**, 106401 (2019).

[12] N. Kozlova, J. Hagel, M. Doerr, J. Wosnitza, D. Eckert, K.-H. Müller, L. Schultz, I. Opahle, S. Elgazzar, M. Richter, G. Goll, H. v. Löhneysen, G. Zwicknagl, T. Yoshino, and T. Takabatake, Phys. Rev. Lett. **95**, 086403 (2005).

[13] D. Aoki, G. Seyfarth, A. Pourret, A. Gourgout, A. McCollam, J. A. N. Bruin, Y. Krupko, and I. Sheikin, Physical Review Letters **116**, 037202 (2016).

[14] H. Aoki, S. Uji, A. K. Albessard, and Y. Ōnuki, Physical Review Letters **71**, 2110 (1993).

[15] G. Bastien, A. Gourgout, D. Aoki, A. Pourret, I. Sheikin, G. Seyfarth, J. Flouquet, and G. Knebel, Physical Re-

view Letters **117**, 206401 (2016).

[16] E. A. Yelland, J. M. Barraclough, W. Wang, K. V. Kamenev, and A. D. Huxley, *Nature Physics* **7**, 890 (2011).

[17] Q. Niu, G. Knebel, D. Braithwaite, D. Aoki, G. Lapertot, G. Seyfarth, J. P. Brison, J. Flouquet, and A. Pourret, *Physical Review Letters* **124**, 086601 (2020).

[18] H. Pfau, R. Daou, S. Lausberg, H. R. Naren, M. Brando, S. Friedemann, S. Wirth, T. Westerkamp, U. Stockert, P. Gegenwart, C. Krellner, C. Geibel, G. Zwicknagl, and F. Steglich, *Physical Review Letters* **110**, 256403 (2013).

[19] H. Pfau, R. Daou, S. Friedemann, S. Karbassi, S. Ghan-nadzadeh, R. Küchler, S. Hamann, A. Steppke, D. Sun, M. König, A. P. Mackenzie, K. Kliemt, C. Krellner, and M. Brando, *Physical Review Letters* **119**, 126402 (2017).

[20] A. Gourgout, A. Pourret, G. Knebel, D. Aoki, G. Sey-farth, and J. Flouquet, *Physical Review Letters* **117**, 046401 (2016).

[21] Z. Zhu, J. Wang, H. Zuo, B. Fauqué, R. D. McDonald, Y. Fuseya, and K. Behnia, *Nature Communications* **8**, 15297 (2017).

[22] C.-L. Zhang, S.-Y. Xu, C. M. Wang, Z. Lin, Z. Z. Du, C. Guo, C.-C. Lee, H. Lu, Y. Feng, S.-M. Huang, G. Chang, C.-H. Hsu, H. Liu, H. Lin, L. Li, C. Zhang, J. Zhang, X.-C. Xie, T. Neupert, M. Z. Hasan, H.-Z. Lu, J. Wang, and S. Jia, *Nature Physics* **13**, 979 (2017).

[23] B. J. Ramshaw, K. A. Modic, A. Shekhter, Y. Zhang, E.-A. Kim, P. J. W. Moll, M. D. Bachmann, M. K. Chan, J. B. Betts, F. Balakirev, A. Migliori, N. J. Ghimire, E. D. Bauer, F. Ronning, and R. D. McDonald, *Nature Communications* **9**, 2217 (2018).

[24] M. Lyu, J. Xiang, Z. Mi, H. Zhao, Z. Wang, E. Liu, G. Chen, Z. Ren, G. Li, and P. Sun, *Physical Review B* **102**, 085143 (2020).

[25] G. Chang, B. Singh, S.-Y. Xu, G. Bian, S.-M. Huang, C.-H. Hsu, I. Belopolski, N. Alidoust, D. S. Sanchez, H. Zheng, H. Lu, X. Zhang, Y. Bian, T.-R. Chang, H.-T. Jeng, A. Bansil, H. Hsu, S. Jia, T. Neupert, H. Lin, and M. Z. Hasan, *Physical Review B* **97**, 041104 (2018).

[26] P. Puphal, C. Mielke, N. Kumar, Y. Soh, T. Shang, M. Medarde, J. S. White, and E. Pomjakushina, *Physical Review Materials* **3**, 024204 (2019).

[27] S. Nakatsuji, N. Kiyohara, and T. Higo, *Nature* **527**, 212 (2015).

[28] K. Kuroda, T. Tomita, M. T. Suzuki, C. Bareille, A. A. Nugroho, P. Goswami, M. Ochi, M. Ikhlas, M. Nakayama, S. Akebi, R. Noguchi, R. Ishii, N. Inami, K. Ono, H. Kumigashira, A. Varykhelov, T. Muro, T. Koretsune, R. Arita, S. Shin, T. Kondo, and S. Nakatsuji, *Nature Materials* **16**, 1090 (2017).

[29] E. Liu, Y. Sun, N. Kumar, L. Muechler, A. Sun, L. Jiao, S.-Y. Yang, D. Liu, A. Liang, Q. Xu, J. Kroder, V. Süß, H. Borrman, C. Shekhar, Z. Wang, C. Xi, W. Wang, W. Schnelle, S. Wirth, Y. Chen, S. T. B. Goennenwein, and C. Felser, *Nature Physics* **14**, 1125 (2018).

[30] N. Morali, R. Batabyal, K. Nag Pranab, E. Liu, Q. Xu, Y. Sun, B. Yan, C. Felser, N. Avraham, and H. Beidenkopf, *Science* **365**, 1286 (2019).

[31] A. Sakai, Y. P. Mizuta, A. A. Nugroho, R. Sihombing, T. Koretsune, M.-T. Suzuki, N. Takemori, R. Ishii, D. Nishio-Hamane, R. Arita, P. Goswami, and S. Nakatsuji, *Nature Physics* **14**, 1119 (2018).

[32] H. Su, X. Shi, J. Yuan, Y. Wan, E. Cheng, C. Xi, L. Pi, X. Wang, Z. Zou, N. Yu, *et al.*, *Physical Review B* **103**, 165128 (2021).

[33] S.-Y. Xu, N. Alidoust, G. Chang, H. Lu, B. Singh, I. Belopolski, S. Sanchez Daniel, X. Zhang, G. Bian, H. Zheng, M.-A. Husanu, Y. Bian, S.-M. Huang, C.-H. Hsu, T.-R. Chang, H.-T. Jeng, A. Bansil, T. Neupert, N. Stro-cov Vladimir, H. Lin, S. Jia, and M. Z. Hasan, *Science Advances* **3**, e1603266 (2017).

[34] P. Puphal, V. Pomjakushin, N. Kanazawa, V. Ukleev, D. J. Gawryluk, J. Ma, M. Naamneh, N. C. Plumb, L. Keller, R. Cubitt, E. Pomjakushina, and J. S. White, *Phys. Rev. Lett.* **124**, 017202 (2020).

[35] H.-Y. Yang, B. Singh, J. Gaudet, B. Lu, C.-Y. Huang, W.-C. Chiu, S.-M. Huang, B. Wang, F. Bahrami, B. Xu, J. Franklin, I. Sochnikov, D. E. Graf, G. Xu, Y. Zhao, C. M. Hoffman, H. Lin, D. H. Torchinsky, C. L. Broholm, A. Bansil, and F. Tafti, *Physical Review B* **103**, 115143 (2021).

[36] J. Gaudet, H.-Y. Yang, S. Baidya, B. Lu, G. Xu, Y. Zhao, J. A. Rodriguez-Rivera, C. M. Hoffmann, D. E. Graf, D. H. Torchinsky, P. Nikolić, D. Vanderbilt, F. Tafti, and C. L. Broholm, *Nature Materials* (2021), 10.1038/s41563-021-01062-8.

[37] L. Ding, J. Koo, L. Xu, X. Li, X. Lu, L. Zhao, Q. Wang, Q. Yin, H. Lei, B. Yan, Z. Zhu, and K. Behnia, *Phys. Rev. X* **9**, 041061 (2019).

[38] B. Fauqué, X. Yang, W. Tabis, M. Shen, Z. Zhu, C. Proust, Y. Fuseya, and K. Behnia, *Phys. Rev. Materials* **2**, 114201 (2018).

[39] R. N. Bhargava, *Physical Review* **156**, 785 (1967).

[40] Z. Zhu, X. Lin, J. Liu, B. Fauqué, Q. Tao, C. Yang, Y. Shi, and K. Behnia, *Physical Review Letters* **114**, 176601 (2015).

[41] J. M. Luttinger, *Physical Review* **119**, 1153 (1960).

[42] H.-Y. Yang, B. Singh, B. Lu, C.-Y. Huang, F. Bahrami, W.-C. Chiu, D. Graf, S.-M. Huang, B. Wang, H. Lin, D. Torchinsky, A. Bansil, and F. Tafti, *APL Materials* **8**, 011111 (2020).

[43] J. Singleton, *Band theory and electronic properties of solids*, Vol. 2 (Oxford University Press, 2001).

[44] D. Shoenberg, *Magnetic oscillations in metals* (Cambridge university press, 2009).

[45] G. Goll, J. Hagel, H. v. Löhneysen, T. Pietrus, S. Wanka, J. Wosnitza, G. Zwicknagl, T. Yoshino, T. Takabatake, and A. G. M. Jansen, *Europhysics Letters (EPL)* **57**, 233 (2002).

[46] P. Nozières, *Eur. Phys. J. B* **6**, 447 (1998).

[47] X. He, C. Zhao, H. Yang, J. Wang, K. Cheng, S. Jiang, L. Zhao, Y. Li, C. Cao, Z. Zhu, S. Wang, Y. Luo, and L. Li, *Phys. Rev. B* **101**, 075106 (2020).

[48] S. Dhar, *J. Magn. Magn. Mater.* **132**, 149 (1994).

[49] G. G. Lesseux, H. Sakai, T. Hattori, Y. Tokunaga, S. Kambe, P. L. Kuhns, A. P. Reyes, J. D. Thompson, P. G. Pagliuso, and R. R. Urbano, *Phys. Rev. B* **101**, 165111 (2020).

Supplemental Material for “Field-Induced Lifshitz Transition in the Magnetic Weyl Semimetal Candidate PrAlSi”

S1. SAMPLES AND METHODS

Single crystals of PrAlSi used in our studies were synthesized using the flux method. The starting materials are high purity chunks of praseodymium, silicon and aluminum, mixed into an alumina crucible. Then, the alumina crucible and quartz wool were placed in a quartz tube, which was sealed under high vacuum, heated to 1100°C at 3°C/min. And holding for 12 h and then the tube was cooled down to 750°C in 100 h and dwells for 2 days. The excess Al flux was removed by centrifuging. To identify the as-grown sample quality of PrAlSi, powder crystal x-ray diffraction (XRD) was used. And, the single crystal XRD has been used to confirm the structure and the orientation of the single crystal. The results revealed the lattice parameters of the specimen are $a = b = 4.22\text{\AA}$, $c = 14.47\text{\AA}$, $\alpha = \beta = \gamma = 90^\circ$ with the tetragonal structure at room temperature. The atomic proportion was determined by energy dispersive x-ray spectroscopy (EDS). The sample for measurements with the dimension of $\sim 2 \times 0.5 \times 0.1 \text{ mm}^3$ and the magnetic field was aligned along c -axis in all measurements. The low-field magnetic transport measurements were performed on an Integra AC (Oxford Instruments) with a 16 T superconducting magnet and a Leiden dilution refrigerator with a 14 T superconducting magnet. Temperature- and field-dependent resistivity measurements were made in the standard four-probe method with a pair of current source (Keithley 6221) and DC-Nanovoltmeter(Keithley 2182A). The high-field magnetic transport measurements were carried out under pulsed magnetic field in Wuhan National High Magnetic Field Center (WHMFC). Golden wires were attached using silver paste on the rectangular sample and the every contact resistance were maintained to be less than 2Ω in the measurements.

The XRD pattern of the PrAlSi single crystal shown in Fig. S1(a) indicating the high quality sample in our measurement and the compositions of the synthesized crystals were analyzed using energy dispersive spectroscopy (EDS), showing in the Fig. S1(b). The temperature-dependent of longitudinal resistivity $\rho_0(T)$ of the PrAlSi single crystal in the absence of an external magnetic field in this work was measured with the current applied along the b -axis ([010]), which showing a typical semimetal character, is presented in the Fig. S1(c). At high temperature, $\rho_0(T)$ displays the metallic behavior with an almost linear temperature dependence from 300 K and develops a small cusp at ferromagnetic transition $T_c = 17.8 \text{ K}$ before further cooling to 2 K. The residual resistivity ratio RRR which is defined as $\rho(300K)/\rho(2K)$ reaches the value of approximate 4.4 in our case. Fig. S1(d) displays the longitudinal magnetoresistivity up to

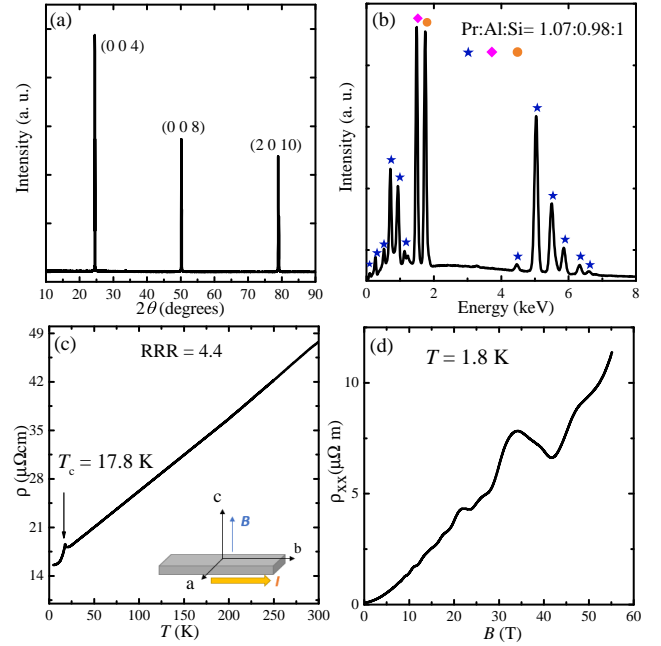


FIG. S1. (a) X-ray diffraction pattern of PrAlSi single crystal. (b) The diagram of the energy dispersive x-ray spectroscopy (EDS). (c) Temperature dependence of electrical resistivity from 2-300 K of the PrAlSi single crystal. The residual resistivity ratio $\rho(300K)/\rho(2K)$ is about 4.4. Inset is the configuration of the measurements. (d) Longitudinal resistivity as a function of magnetic field up to 55 T at 1.8 K.

$1140 \mu\Omega\text{cm}$ under high magnetic field.

S2. RAW DATA OF THE FIELD DEPENDENCE OF MAGNETORESISTANCE AND AVERAGE MOBILITY

The temperature dependence of magnetoresistance of single crystal PrAlSi were measured under static field up to 14 T (Leiden dilution refrigerator) in Fig. S2(a) and up to 16 T (Oxford Instruments) in Fig. S2(b), respectively. Positive and unsaturated magnetoresistance and evident SdH oscillations under low temperature above 3 T are visible until up to 35 K in our measurements. The inset in (a) is the fitting result of $\text{MR} = \mu_{ave} B^2$ guided by the violet line and the obtained average mobility is $0.26 \text{ m}^2/\text{Vs}$.

S3. DETAILS OF FFT ANALYSIS

As mentioned above, the SdH QOs frequencies are discriminative with only one dominating frequency F_1 (43 T) below 14.5 T and another two higher frequencies F_2 (62 T) and F_3 (103 T) existing under higher field. We selected different low magnetic field ranges to analyze the FFT from the result of MR showing in Fig. S3. The FFT results accord with the discussion in Fig. 2, which

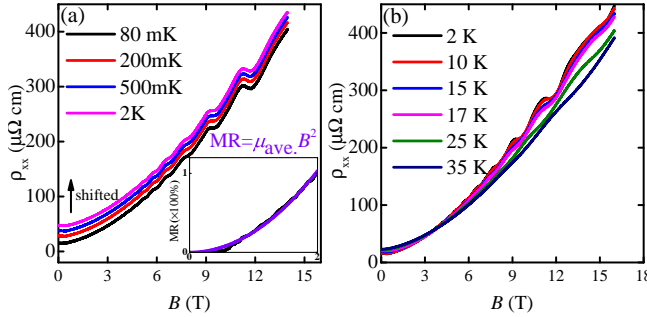


FIG. S2. (a) The temperature-dependent magneto resistivity ρ_{xx} (shifted) measured from $T = 80$ mK to 2 K with magnetic field up to 14 T, the inset is the fitting result of the equation $MR = \mu_{ave} B^2$ with $\mu_{ave} = 0.26$ m^2/Vs . (b) ρ_{xx} with the temperature variation from 2 K to 35 K as magnetic field up to 16 T.

indicating only one domain frequency under the critical magnetic field 14.5 T and the FFT peak becomes widely at 15 T and involves into another peaks when magnetic field increasing up to 20 T eventually. This FFT analysis clearly shows the frequency variation as the function of magnetic field, we consider that 14.5 T (labelled with B^*) is indeed a critical point and the conclusion is well agreed with the two-band fitting of Hall resistivity in main text.

S4. THE LIFSHITZ-KOSEVICH (LK) THEORY

As is known, the oscillatory part of magnetoresistance can be described by the LK formula[1] which is: $\Delta\rho = \sum_i A_i R_{Ti} R_{Di} \cos[2\pi(\frac{F_i}{B} - \delta_i)]$, where i is the number of Fermi pocket, A_i are prefactors, F_i are the oscillatory frequencies and δ_i are the phase factors. The $R_{Ti} = \alpha T m_i^* / B \sinh[\alpha T m_i^* / B]$ and $R_{Di} = \exp[\alpha T D_i m_i^* / B]$ are the thermal and scattered damping factors, where $\alpha = 2\pi^2 k_B m_e / e\hbar \simeq 14.69$ T/K, m^* is the cyclotron mass and T_{Di} is the Dingle temperature.

S5. FIELD DEPENDENCE OF MASS FOR THE F_1

As described in main text, the LT occurs around $B^* = 14.5$ T with the disappearance of a lower SdH frequency $F_1 = 43$ T. It's naturally to study the evolution of this Fermi pocket so that we extracted the effective mass as a function of magnetic field below B^* from the temperature dependence of the SdH oscillatory components at different fields as shown in the Fig. S4. We can extract m^* from the SdH peaks directly because it relates to the temperature damping factor which is evident reflecting in the SdH oscillation component showing in Fig. S4(a). In addition, the effective masses of the Fermi pockets mentioned in Fig. 2, which were extracted from the amplitude of temperature-dependent FFT spectra,

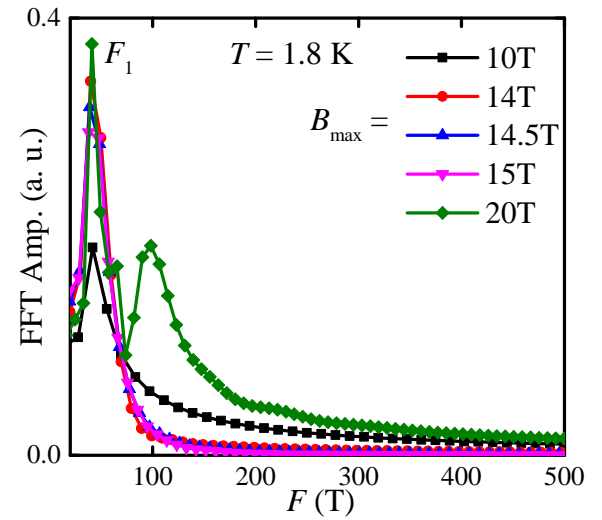


FIG. S3. The FFT analysis spectrum of MR measured in pulsed field with selected magnetic field maximum nearby the B^* .

are plotted in Fig. S4(b).

S6. QUANTUM OSCILLATION PHASE FACTOR ANALYSIS FOR F_1

In order to pin down the property of the topological state in PrAlSi, the Landau level (LL) index fan diagram,

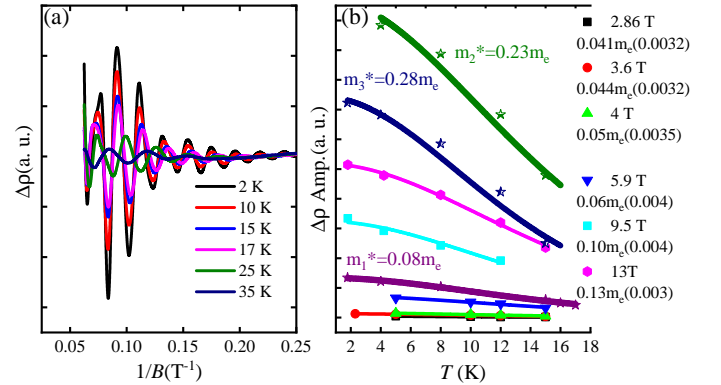


FIG. S4. (a) The SdH oscillatory component as a function of $1/B$ after subtracting the smoothed background from 2 K to 35 K measured under static field with magnetic field up to 16 T. (b) Effective masses of F_1 as a function of magnetic field below B^* extracted from the temperature-dependent SdH amplitude of peaks by fitting with the damping factor in the LK function are summarized in the Fig. 2(c). Besides, the cyclotron mass m^* of F_1 was extracted by fitting the FFT amplitude of SdH oscillations (Fig. 2(a)) to the temperature damping factor of the LK equation from 5.7 T to 14.5 T, and the same method for F_2 and F_3 with field from 14.5 T to 55 T.

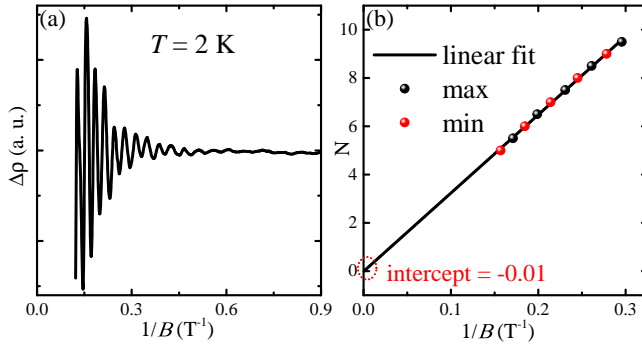


FIG. S5. (a) $\Delta\rho$ as the function of B^{-1} at indicated temperature. (b) Landau level fan diagram of F_1 extracted from $\Delta\rho$ and the line indicates the linear fitting to the data. The solid circles represent the maxima and minima of $\Delta\rho$, respectively.

which could manifest the nontrivial φ_B in Weyl system, is much essential. The oscillatory component $\Delta\rho$ at 2 K under static field is obtained by subtracting the background and plotted as the function of $1/B$ in Fig. S5(a). An apparent simple pattern here is in accordance with the discussion of Fig. 1 in main text indicating the single main frequency under low magnetic field range in QOs pattern. According to the LK formula:

$$\Delta\rho \sim \frac{\lambda T}{\sinh(\lambda T)} e^{-\lambda T_D} \cos[2\pi(\frac{F}{H} - \frac{1}{2} + \delta)] \quad (\text{S1})$$

Here, the phase factor is $\delta - \frac{1}{2} = \frac{\varphi_B + \varphi_D}{2\pi} - \frac{1}{2}$, where φ_B is Berry phase and φ_D equals $\pm\frac{1}{8}$ which depends on the cross-section extremum with maximal or minimal for 3D cases. Fig. S5(b) displays the Landau level(LL) fan diagram for the fundamental frequency F_1 . Here, the minimum $\Delta\rho$ (red) is integer indices and the maximum $\Delta\rho$ (black) is half-integer indices. All points are well linearly fitting and we extrapolate $1/B$ to zero and obtain the intercept is $-0.01 = \delta - \frac{1}{2}$, indicating a π Berry phase and non-trivial topological state of the F_1 in PrAlSi single crystal.

S7. TWO-BAND FITTING FOR THE MAGNETORESISTIVITY ρ_{xx} AND HALL CONDUCTIVITY σ_{xy}

ρ_{xx} and σ_{xy} in our case can be described by the two-band model:

$$\rho_{xx} = \frac{1}{e} \frac{(n_h\mu_h + n_e\mu_e) + \mu_h\mu_e(n_e\mu_h + n_h\mu_e)B^2}{(n_h\mu_h + n_e\mu_e)^2 + \mu_h^2\mu_e^2(n_h - n_e)^2B^2} \quad (\text{S2})$$

$$\sigma_{xy} = eB \left(\frac{n_h\mu_h^2}{1 + \mu_h^2B^2} - \frac{n_e\mu_e^2}{1 + \mu_h^2B^2} \right) \quad (\text{S3})$$

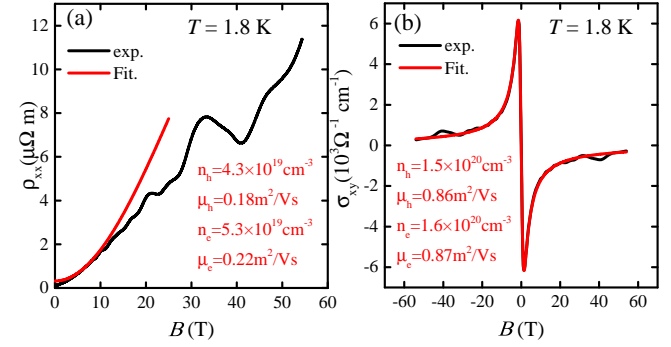


FIG. S6. Magnetoresistivity (a) and Hall conductivity (b) of PrAlSi at 1.8 K. The black solid line is the experimental data and the red solid line is the fitted curve with two-band model, respectively.

Here, $n_h(n_e)$ and $\mu_h(\mu_e)$ are carrier concentration and mobility for the holes (electrons), respectively. The fitted result of magnetoresistivity ρ_{xx} with the parameters identical with the main text shows a good fit in low field range up to B^* shown in Figure. S6(a) in red, while the experimental curve is in black.

The fitted result of Hall conductivity σ_{xy} indicates carrier concentration are $n_h = 1.5 \times 10^{20} \text{ cm}^{-3}$ ($n_e = 1.6 \times 10^{20} \text{ cm}^{-3}$) and the corresponding mobilities are $\mu_h = 0.86 \text{ m}^2/\text{Vs}$ ($\mu_e = 0.81 \text{ m}^2/\text{Vs}$). The field dependence of Hall conductivity shows a sharp rise in the low fields and slowly decrease as the field is increased. The fitting is tricky and a little change in the parameters would not change the fitting result, especially in the high-field range. So we fit the Hall resistance which has much better shape for the fitting, giving more convincing results. Besides, the obtained carriers 1.5×10^{20} (1.6×10^{20}) cm^{-3} for holes (electrons) lead to a mobility of $0.17 \text{ m}^2/\text{Vs}$ at zero field, which is quite distinct from the fitting results of $\sim 0.9 \text{ m}^2/\text{Vs}$.

S8. THE COMPARISON OF HALL RESISTIVITY WITH CEBIPT

In CeBiPt, LT promotes carrier density from $7.2 \times 10^{17} \text{ cm}^{-3}$ to $9.2 \times 10^{17} \text{ cm}^{-3}$, increased by 28%. The change of PrAlSi is mainly in mobility beyond after LT, with 75% for holes and 27% for electrons. The large drop of mobility is most likely due to the increase of inter-bands scattering because of more pockets present after LT and also the increase of mass of the pockets. The drops in mobility may result in the downward of MR above LT in the Fig. 1(a). The sub-linear Hall resistance is single-band behavior in CeBiPt[2], while it is a multi-band behavior in PrAlSi and has two-order higher carriers concentration and mainly change its mobility. Thus, one can clearly observe the linearity change of Hall resistance in CeBiPt, while smooth evolution of Hall resistivity and an evident deviation in first derivative of Hall resistivity in the cur-

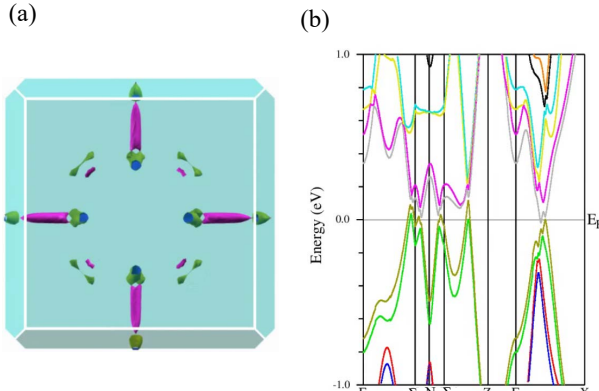


FIG. S7. The first-principle calculation results. (a) The calculated Fermi surface and (b) band structure of the PrAlSi.

rent case. The same feature is that no sudden change in Hall resistance occurs during LT.

S9. INTERNAL FIELD AND EXTERNAL FIELD

PrAlSi is a ferromagnet with the $T_c = 17.8$ K (Fig. S1(c)). We considered its demagnetization factor and external field to infer the internal field which exerts on carriers. The internal field $B_{int} = \mu_0 H_{ext} + \mu_0(1-n)M$, where n is the demagnetization factor. According to the report [3], $n = 0.77$ of our rectangular sample is obtained by fitting the shape factor into the given function. $\Delta B = B_{int} - B_{ext} = 0.23\mu_0 M_{exp} = 0.46$ T, here $\mu_0 = 1.257 \times 10^{-6} H/m$.

S10. THEORETICAL CALCULATION

The theoretical calculation was carried out with WIEN2k which is based on the density functional theory (DFT) based linearized augmented plane wave (LAPW) method[4]. We used the Perdew-BurkeErnzerhof (PBE) generalized gradient approximation (GGA)[5] form of the

exchange correlation functional. The RKmax was set to 5 which is determined by the smallest atom Si[4]. The results are for the effective Hubbard U of 6 eV by taking the on-site correlation using the DFT+U approximation for the f state of Pr. The spin orbit coupling was included in second variation of the calculation. The calculated results are consistent with the reported[6], shown in the S7, plotted by XcrysDen[7]. Along Γ -X direction in the S7(a), the small pockets located the sides of the direction have 8 pockets, which could be the F_1 . The calculated band structure shown in the S7(b) is also well consistent with the reported. Along Γ -X direction, the bands are

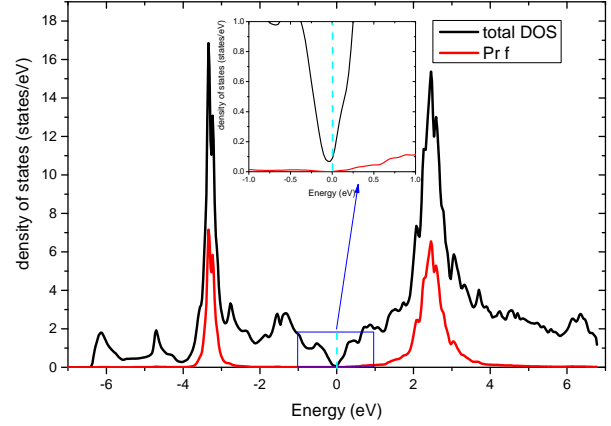


FIG. S8. The total density of states and the density of states (DOS) of f orbit.

shallow and could be source of the instability during the LT process.

S11. THE DOS OF PR F ELECTRON

The Fig. S8 shows the total density of states and the density of states (DOS) of f orbit from Pr in the energy scale of -7 to 7 eV. And the inset shows the enlarged part for the energy scale of -1 to 1 eV. All the f electrons of Pr are clearly below Fermi level and do not contribute to the conductivity on the Fermi surface. So we will not expect $f-c$ (c -conduction electrons) hybridization in the system.

[1] D. Shoenberg, *Magnetic oscillations in metals* (Cambridge university press, 2009).
[2] N. Kozlova, J. Hagel, M. Doerr, J. Wosnitza, D. Eckert, K.-H. Müller, L. Schultz, I. Opahle, S. Elgazzar, M. Richter, G. Goll, H. v. Löhneysen, G. Zwicknagl, T. Yoshino, and T. Takabatake, Phys. Rev. Lett. **95**, 086403 (2005).
[3] A. Aharoni, Journal of Applied Physics **83**, 3432 (1998).
[4] P. Blaha, K. Schwarz, F. Tran, R. Laskowski, G. K. H. Madsen, and L. D. Marks, The Journal of Chemical Physics **152**, 074101 (2020).
[5] J. P. Perdew, K. Burke, and Y. Wang, Physical Review B **54**, 16533 (1996).
[6] H.-Y. Yang, B. Singh, B. Lu, C.-Y. Huang, F. Bahrami, W.-C. Chiu, D. Graf, S.-M. Huang, B. Wang, H. Lin, D. Torchinsky, A. Bansil, and F. Tafti, APL Materials **8**, 011111 (2020).
[7] A. Kokalj, Journal of Molecular Graphics and Modelling **17**, 176 (1999).